Frontiers of Information Technology & Electronic Engineering
www.jzus.zju.edu.cn; engineering.cae.cn; www.springerlink.com
ISSN 2095-9184 (print); ISSN 2095-9230 (online)
E-mail: jzus@zju.edu.cn

Spatial fading channel emulation for over-the-air testing of millimeter-wave radios: concepts and experimental validations*

Wei FAN[†‡1], Lassi HENTILÄ[2], Pekka KYÖSTI[2,3]

[1]*Antenna Propagation and Millimeter-wave Systems (APMS) Section, Department of Electronic Systems, Aalborg University, Aalborg 9220, Denmark*

[2]*Keysight Technologies Finland Oy, Oulu 90014, Finland*

[3]*Centre for Wireless Communications, University of Oulu, Oulu 90014, Finland*

[†]E-mail: wfa@es.aau.dk

Received Sept. 17, 2020; Revision accepted Jan. 6, 2021; Crosschecked Mar. 2, 2021

Abstract: Millimeter-wave (mmWave) communication is regarded as the key enabling component for fifth-generation (5G) cellular systems due to the large available spectrum bandwidth. To make mmWave new radio (NR) a reality, tremendous efforts have been exerted from the industry and academia. Performance evaluation of mmWave NR is a mandatory step and the key to ensuring the success of mmWave 5G deployment. Over-the-air (OTA) radiated method of testing mmWave NR in laboratory conditions is highly attractive, since it facilitates virtual field testing of mmWave devices in realistic propagation conditions. In this paper, we first discuss the need for and challenges in OTA measurement of mmWave 5G NR under fading channel conditions. After that, two promising candidate solutions, i.e., wireless cable and multi-probe anechoic chamber (MPAC), are detailed. Their principles, applicability for mmWave NR, and main challenges are discussed. Furthermore, preliminary experimental validation results in a frequency range 2 anechoic chamber are demonstrated for the wireless cable and MPAC methods at 28 GHz.

Key words: Spatial channel model; Over-the-air (OTA) testing; Wireless cable method; Multi-probe anechoic chamber (MPAC) method; FR2 validation

https://doi.org/10.1631/FITEE.2000484 **CLC number:** TN928

1 Introduction

Millimeter-wave (mmWave) communication is seen as the key enabling technology to achieve high data rate transmission (Rappaport et al., 2013; Shafi et al., 2017; Guan et al., 2019a, 2019b). To make mmWave fifth-generation (5G) new radio (NR) (i.e., the global 5G standard) a success, tremendous efforts have been exerted from academia, industry, and government laboratories in the past few years. Many 5G field trials and test-bed platforms have been reported by key industrial and academic players (Shafi et al., 2017), wherein the objective is to demonstrate and validate whether key performance indicators (KPIs) for 5G systems can be met in various representative real-world deployment scenarios. However, field trials are expensive and uncontrollable. If systems fail in field trials, it is difficult and complicated to identify the root cause, due to the lack of controllable and repeatable testing environments.

For sub-6 GHz antenna systems, accessible antenna connectors are typically implemented for cable-conducted testing purposes. However, it is predicted that conducted testing will no longer be

‡ Corresponding author

* Project supported by the InnoExplorer Project Funded by Innovation Fund Denmark (No. 20199122-00089A)

ORCID: Wei FAN, https://orcid.org/0000-0002-9835-4485

applicable for mmWave NRs, due to the lack of antenna connectors (Chen, 2014; Chen et al., 2009; Rumney, 2016; Qi et al., 2017; Fan et al., 2018b; Wang et al., 2019; Li et al., 2020; Qiao et al., 2020; Zhang YS et al., 2020). Meanwhile, mmWave antennas are small, highly integrated units (e.g., antenna on chip or antenna in package), and possibly, with a massive antenna count. Therefore, mmWave NR testing will move exclusively to over-the-air (OTA) radiated modes using device antennas as the direct interface with the test system. This also allows the possibility to take into consideration mmWave antenna systems in the performance testing.

Historically, OTA testing has been used to evaluate radio performance of antenna systems. OTA testing of single-antenna user terminals was standardized more than a decade ago (CTIA, 2018). OTA testing for sub-6 GHz Long-Term Evolution (LTE) multiple-input multiple-output (MIMO) terminals has been standardized in the Cellular Telecommunications and Internet Association (CTIA) and the Third Generation Partnership Project (3GPP) standards, wherein the multi-probe anechoic chamber (MPAC) and the radiated two-stage (RTS) methods have been selected and standardized (CTIA, 2017; Wang et al., 2019; Li et al., 2020). Meanwhile, the automotive industry started to adopt OTA testing solutions for sub-6 GHz MIMO systems to ensure reliable wireless communication in dynamic vehicle-to-vehicle and vehicle-to-infrastructure scenarios (Nilsson et al., 2015; Ji et al., 2020). Strong efforts have been taken in 3GPP recently to standardize the test methodology for verification of multi-antenna reception performance of NR user equipment (UE) (3GPP, 2020). For frequency range 1 (FR1), i.e., frequency range of 450–6000 MHz, the two-dimensional (2D) MPAC method is the reference methodology, while the RTS method is selected as the harmonized methodology. For FR2, which corresponds to the frequency range of 24.25–52.6 GHz, the three-dimensional (3D) simplified MPAC test setup is selected as the reference methodology.

One essential step in the research and development stage is to validate 5G radios under ideal and clean RF propagation channel conditions. For example, the plane wave condition is adopted as the default reference for characterization of the antenna and the radio frequency (RF) transceiver, including antenna radiation pattern, transmitter and receiver radiation performance, and antenna array calibration. Several strategies to mimic the plane wave testing condition, e.g., direct far-field chamber, compact antenna testing range, plane wave generator, and near-field to far-field transformation techniques, have been reported (Keysight Technologies, 2018). It is also of great importance to optimize and validate the device performance in real-world conditions, i.e., under faded and subject to interference channel conditions with multiple cells, users, and radio access technologies. Therefore, channel emulators (CEs), which are typically used to emulate the radio channel between the transmitter (TX) and the receiver (RX), are extensively used for end-to-end real-world performance testing for wireless devices and base stations in the labatory (Fan et al., 2018a). It would be desirable to develop cost-effective OTA testing methodologies in laboratory conditions, which makes it possible to achieve virtual field testing purposes of mmWave devices in realistic conditions. This enables the testing of all the mmWave 5G KPIs in various scenarios (including 5G friendly or 5G hostile scenarios) reproduced in a controllable way. By doing so, the engineer has the possibility to quickly verify the performance of the mmWave NR and to quickly test how changes in hardware and software design affect the NR system's performance. The goal is to develop an OTA testing methodology suitable to evaluate mmWave NR in a realistic, reliable, repeatable, and cost-efficient way in laboratory conditions, thereby ensuring timely and efficient development and optimization of mmWave devices. There is a strong need for a standard and cost-effective testing solution from the industry and government laboratories, since mmWave OTA testing is required for the success of mmWave 5G deployment.

In this work, the main focus is on spatial fading channel emulation for the OTA testing of mmWave radios and its validation in a practical FR2 anechoic chamber. Validation of spatial fading channel emulation in FR1 has been extensively discussed in the literature (Yu et al., 2014; CTIA, 2017; Zhang FC et al., 2021). However, no work has been reported on validation in the FR2 chamber. There are some practical differences in the processes of validation in the FR1 and FR2 chambers. The probe antennas and measurement antennas are more directive at the FR2. The virtual array, which is used to estimate the

emulated channel spatial profile in the chamber, will be more difficult to form with the mechanical positioner, as the wavelength at the FR2 is much smaller. The channel emulation at the FR2 is also more complicated, which involves frequency up-and-down conversion for the sub-6 GHz CE. To bring mmWave OTA testing from theory into practice, we also must ask to what extent the theoretical analysis can be maintained in realistic testing setups. Most work on mmWave OTA testing in spatial fading channels presented in the literature is limited to theoretical analysis via numerical simulations, clearly lacking experimental validation in practical mmWave OTA setups (Fan et al., 2018b; Wang et al., 2019; Li et al., 2020). In this paper, we experimentally validate the wireless cable method and the MPAC method in a practical setup for mmWave NR testing. We first discuss two OTA methods that are capable of emulating spatial fading channels. Two simple strategies to achieve wireless cable connection for mmWave radios, i.e., using antenna polarization discrimination and pattern discrimination, are proposed. Their applicability to and limitations in the context of mmWave radios are discussed. The main contributions of the study are as follows:

1. The main work is spatial fading channel emulation for OTA testing of mmWave radios and its experimental verification in an actual FR2 anechoic chamber, which has not been reported in the literature yet.

2. The methods of using antenna pattern diversity and polarization diversity are proposed to achieve wireless cable connection for mmWave radios, and this is also experimentally validated.

2 Wireless cable method

2.1 Principle

In the cable conducted testing setup as shown in Fig. 1a, the output ports of the CE are directly coupled to the antenna ports of the MIMO device with coaxial RF cables. In other words, RF cables are used to directly guide the testing signals to the respective antenna ports, bypassing (most likely, internal) antennas from the MIMO device. A graphical representation of an LTE handset supporting a multi-band 4×4 MIMO is shown in Fig. 2. As we can see, it becomes increasingly problematic for the traditional cable conducted setup, as the number of receiver antennas and the frequency bands continue to increase for future UEs.

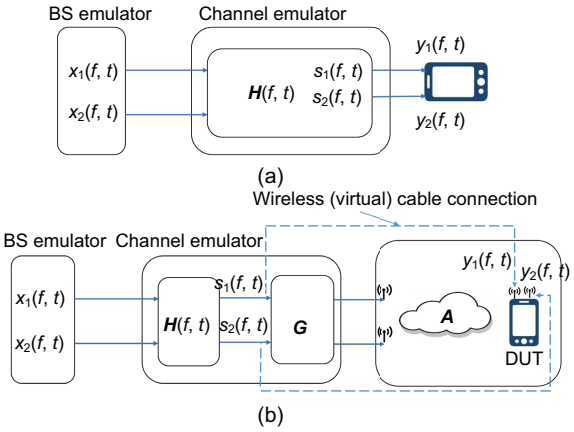

Fig. 1 Illustration of the conducted cable setup (a) and the wireless cable setup for mobile handsets supporting 2×2 MIMO systems (b)

BS: base station; MIMO: multiple-input multiple-output

Fig. 2 A graphical representation of a commercial LTE mobile handset supporting multi-band 4×4 MIMO systems

LTE: long-term evaluation; MIMO: muliple-input multiple-output

The wireless (virtual) cable method, which aims to achieve coaxial cable functionality (i.e., signals guided to the respective antenna ports with high isolation to cross-talk links) over-the-air, has attracted great research attention recently from both industry and academia (Jing et al., 2016; Rumney et al., 2016; Schirmer et al., 2016; Zhang FC et al., 2021). As illustrated in Fig. 1b, the basic concept is that the measured static transfer function matrix from the

probe antenna ports to the device under test (DUT) antenna ports can be calibrated in the CE.

In the cable conducted setup as illustrated in Fig. 1a, the signal model can be written as follows (ignoring the noise at the receiver side and assuming ideal transmission, i.e., balanced power and no cross-talk among the RF cables):

$$\boldsymbol{y}(f,t)=\boldsymbol{s}(f,t)=\boldsymbol{H}(f,t)\boldsymbol{x}(f,t), \tag{1}$$

where we have the time-variant channel frequency response (CFR) matrix $\boldsymbol{H}(f,t)\in\mathbb{C}^{N\times M}$ between M transmitter antenna ports and N receiver antenna ports, the received signal vector $\boldsymbol{y}(f,t)\in\mathbb{C}^{N\times 1}$ at the N receiver antenna ports, the transmitted signal vector $\boldsymbol{x}(f,t)\in\mathbb{C}^{M\times 1}$ at the M transmitter antenna ports, and the testing signal vector $\boldsymbol{s}(f,t)\in\mathbb{C}^{N\times 1}$ to be directed to the N receiver antenna ports.

In the wireless cable illustrated in Fig. 1b, the signal model can be written as follows:

$$\begin{aligned}\boldsymbol{y}(f,t)&=\boldsymbol{A}\boldsymbol{G}\boldsymbol{s}(f,t)=\boldsymbol{A}\boldsymbol{G}\boldsymbol{H}(f,t)\boldsymbol{x}(f,t)\\&=\boldsymbol{H}(f,t)\boldsymbol{x}(f,t),\end{aligned} \tag{2}$$

where $\boldsymbol{A}\in\mathbb{C}^{N\times K}$ is the transfer function matrix between K probe antenna ports and N receiver antenna ports to be measured, and $\boldsymbol{G}\in\mathbb{C}^{K\times N}$ is the compensation matrix to approximate $\boldsymbol{A}\boldsymbol{G}=\boldsymbol{I}_{N\times N}$. The actual channel model implemented in the CE is $\boldsymbol{H}_{\mathrm{CE}}(f,t)=\boldsymbol{G}\boldsymbol{H}(f,t)$. The main challenge of the wireless cable method is efficiently obtaining the static transfer function matrix in the calibration stage for commercial MIMO devices.

From Eq. (2), it is clear that to ensure that the target $\boldsymbol{A}\boldsymbol{G}=\boldsymbol{I}_{N\times N}$ can be approximated, $K\geq N$ should be met. For a receiver with digital structure, i.e., one RF chain per antenna radiating element, the number of probe antennas (thereby, the corresponding CE RF interface ports) should be no smaller than the number of DUT antennas. For a receiver with analog or hybrid structure, i.e., one RF chain corresponding to a set of radiating elements, the number of probe antennas should be no smaller than the number of DUT RF chains. Furthermore, the transfer function matrix $\boldsymbol{A}$ should be invertible (well-conditioned), static (i.e., non-adaptive to received signals), and preferably frequency independent. Moreover, DUT antennas are bypassed in the wireless cable setup (as in the conducted testing setup); i.e., DUT antennas are not included in the testing by default. However, their antenna patterns, if known, can be indirectly considered in the CE during testing.

2.2 Application for sub-6 GHz radios

For sub-6 GHz mobile handsets and automobiles, DUTs are typically equipped with a few antennas, with unknown antenna designs and locations. The antenna radiation pattern is often quasi-omnidirectional with unknown polarization. Furthermore, in a compact measurement setup, multiple propagation paths exist between the probe antennas and DUT antennas. Consequently, the transfer function matrix $\boldsymbol{A}$ is an unknown non-identity matrix. Therefore, it must be measured and calibrated in the CE to achieve wireless cable connection.

Many strategies have been reported in the literature to obtain $\boldsymbol{A}$, depending on the available output information from the DUT. It has been shown (Yu et al., 2014; Rumney et al., 2016) that $\boldsymbol{A}$ can be directly calculated based on the knowledge of complex antenna patterns of the DUT. This method, however, requires a large anechoic chamber for far-field antenna pattern measurement and support from a special chip-set to report DUT complex antenna patterns in a non-intrusive manner. In Schirmer et al. (2016), it has been demonstrated that $\boldsymbol{A}$ can be directly estimated via channel estimation algorithms, e.g., using pilot sequence. This idea, however, might be supported only by base station (BS) type DUT where transmitted signals can be designed and therefore known. In Zhang FC et al. (2021), based on the value of the received reference signal received power (RSRP) per DUT antenna port, a calibration method has been proposed to determine $\boldsymbol{A}$. The method is highly attractive since the testing can be performed in a small RF shielded enclosure. The method is then extended for high-order MIMO DUT in Zhang FC et al. (2021), with a closed-form calibration method.

2.3 Applicability for mmWave NR

For mmWave mobile handsets, the antenna designs are widely different from those used for sub-6 GHz systems. The mmWave radios rely heavily on beamforming capability to improve the signal-to-noise ratio (SNR) of the link signal and track the dominant propagation paths in the dynamic channel.

Therefore, DUT antenna patterns are directive and adaptive. As discussed, the transfer matrix $\boldsymbol{A}$ should remain static to establish the wireless cable connection. As a result, the antenna patterns on the DUT should be fixed during testing (i.e., the so-called beam-locked mode).

It is defined in 3GPP Release 15 (Muruganathan et al., 2018) that for a 2×2 MIMO system, spatial multiplexing is achieved using the polarization domain, i.e., one data stream per orthogonal polarization. High-order MIMO systems will be defined in the future using the multi-antenna domain. The unique features of mmWave antennas open up new possibilities to achieve wireless cable connections. A straightforward way to achieve wireless cable connection is to design the transfer function matrix $\boldsymbol{A}$ such that $|\boldsymbol{A}| = \boldsymbol{I}$ can be directly approximated in the multi-probe setup, without the need to compensate for it in the CE. As illustrated in Fig. 3a, if the DUT can form widely separated directive beam patterns, each toward a directive and direction-aligned probe antenna, we can achieve cable-like connection over-the-air via antenna pattern discrimination. Alternatively, polarization discrimination is another way to achieve virtual cable connection for 2×2 MIMO systems, as illustrated in Fig. 3b. The wireless cable can be directly achieved through the adoption orthogonality between two cross-polarized components, whereby two wireless cable connections can be achieved.

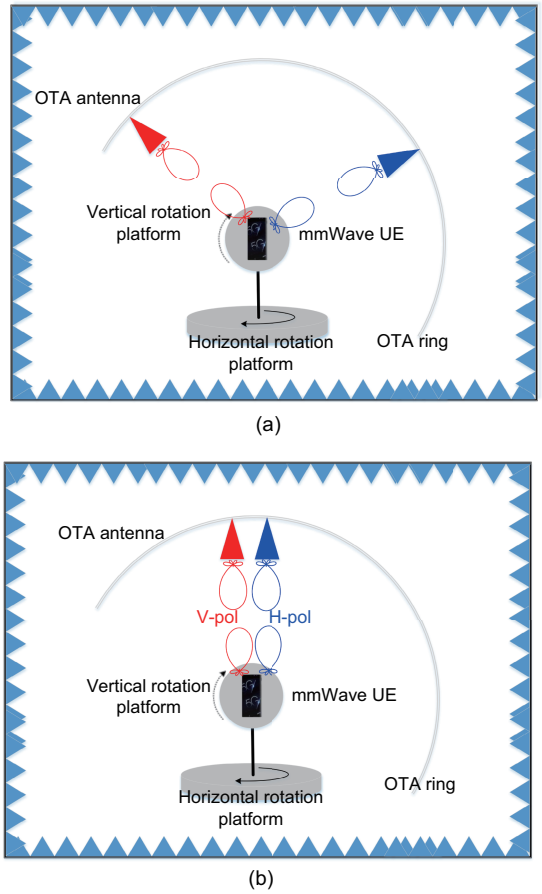

Fig. 3 Illustration for achieving wireless cable connection via antenna pattern discrimination (a) and antenna polarization discrimination (b)

mmWave: millimeter-wave; OTA: over-the-air; UE: user equipment

As explained, the basic idea of the wireless cable concept is that we need to determine the transfer function matrix $\boldsymbol{A}$ and then calibrate it. In some special cases, we can directly design the transfer function matrix $\boldsymbol{A}$ such that $|\boldsymbol{A}| = \boldsymbol{I}$ can be approximated in the multi-probe setup. Therefore, there is no need to calibrate it out. Two schemes proposed in this study, i.e., polarization discrimination and antenna pattern discrimination, are two examples to approximate this special condition $|\boldsymbol{A}| = \boldsymbol{I}$. However, to exploit the antenna pattern discrimination scheme, the DUT must be able to form widely separated directive beam patterns, each toward a directive and direction-aligned probe antenna. To exploit the polarization discrimination scheme, the DUT must support two orthogonal polarizations, each aligned with the polarization of one probe antenna. This strategy is not generic for any DUT and in any multi-probe setup. For small mmWave user terminals, it might not be practical to design many widely separated beams due to design limitations. Regarding the polarization discrimination case, it is limited only to 2×2 MIMO systems and MIMO handsets with two orthogonal linearly polarized antenna designs. Therefore, the transfer function matrix $\boldsymbol{A}$ might not approximate an identity matrix in practice in a general sense. The more general calibration method, which can determine the transfer function matrix $\boldsymbol{A}$ without relying on DUT antenna radiation properties and multi-probe setup, is therefore more generic to achieve wireless cable connection. A generic scheme to achieve wireless cable connection for any DUT has been proposed in Fan et al. (2017) for 2×2 MIMO and in Zhang FC et al. (2021) for high-order MIMO devices. The method requires monitoring of the average received power per DUT antenna port in the calibration stage and has been validated for sub-6 GHz devices. So far, it has not

been validated for commercial mmWave devices due to the lack of experimental facilities, and this part will be addressed in future work.

2.4 Experimental validation

2.4.1 Measurement setup

The system diagram of the measurement setup for validating the wireless cable method is shown in Fig. 4. A vector network analyzer (VNA) is used to record CFRs S_{21} and S_{41}. A sub-6 GHz CE is extended to the mmWave CE using frequency mixers to up- and down-convert the signal frequency (Fan et al., 2018a). An analog signal generator is used to generate the local oscillator frequency. The frequency conversion is marked in red texts in Fig. 4. The analog signal generator, VNA, and CE are synchronized using the 10 MHz reference connection.

For validation purpose, time-invariant channel impulse responses (CIRs) are loaded in the CE. Here, $h_{11}(\tau)$ is a single tap channel with path power 0 dB and $\tau = 0$ ns, while $h_{22}(\tau)$ is also a single tap channel with path power 0 dB and $\tau = 935$ ns. Furthermore, $h_{21}(\tau)$ and $h_{12}(\tau)$ are disabled in the CE. The different tap delay values in $h_{11}(\tau)$ and $h_{22}(\tau)$ are intentionally designed to check how well wireless cable connections are achieved. For ideal wireless cable connections, $h_{11}(\tau)$ and $h_{22}(\tau)$ can be recorded only in the first (i.e., S_{21} measurement) and second (i.e., S_{41} measurement) DUT antennas, respectively, with no cross-talk with other DUT antennas. Therefore, we can easily check how well the wireless cable connection is established by comparing the power values at the two different delay taps on each DUT receiver antenna.

A graphical representation of the measurement setup inside the anechoic chamber for the wireless cable method using the polarization discrimination scheme and the antenna pattern discrimination scheme are shown in Figs. 5 and 6, respectively. The measurement was done in an FR2 anechoic chamber located at Keysight Technologies, Finland. Two dual-polarized probe antennas on a ring (each with two polarization feed antenna ports) were used. Two linearly polarized standard gain horn antennas operating at 28 GHz were used to mimic the two beams formed by the mmWave DUT. According to the literature (3GPP, 2019), the reference antenna under test for the FR2 UE shall be a directive antenna, in which the half-power beamwidth (HPBW) of the reference antenna at 28 GHz in the H-plane ranges from around 15° to 30°. The HPBW of the horn antenna in the measurement is around 20°, which is suitable for mimicking the FR2 UE beams.

The DUT antennas were placed on a turntable in the center of the chamber, with a distance of around 1 m to the probe antennas on the ring. To enable the polarization discrimination scheme, the horizontal polarization (H-pol) port on one probe antenna and the vertical polarization (V-pol) port on the other probe antenna are connected to the mmWave CE output ports. At the DUT side, one

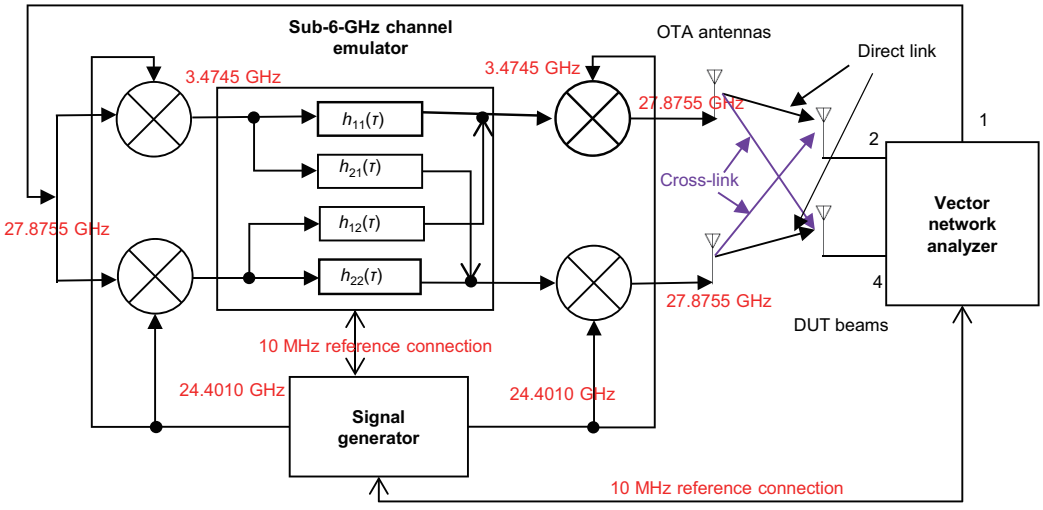

Fig. 4 System diagram for the wireless cable method validation setup

DUT: device under test; OTA: over-the-air. References to color refer to the online version of this figure

DUT antenna is aligned to the V-pol of the probe antenna, while the other DUT antenna is rotated 90° to align with the H-pol of the other probe antenna, as shown in Fig. 5. To mimic the wireless cable connection using the antenna pattern discrimination scheme, the probe configuration and the DUT antenna configuration are shown in Fig. 6. Basically, the probe antennas are widely separated to minimize cross-talks, and the two DUT antennas are steered toward the respective probe antennas. As seen in Fig. 6, both the probe antennas and the measurement antennas are aligned in the V-pol direction, which indicates that only antenna pattern discrimination is used in the measurement. In principle, we can further reduce the cross-talk using both the antenna pattern and the polarization discrimination scheme for 2×2 MIMO systems.

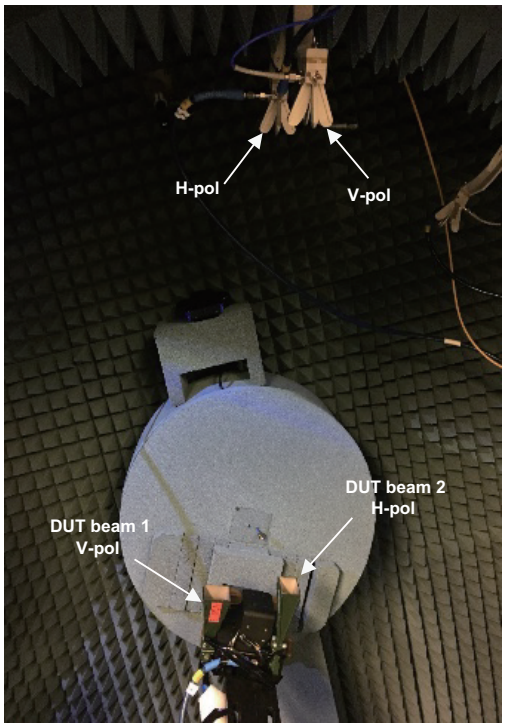

Fig. 5 Measurement setup for the wireless cable method using the polarization discrimination scheme
DUT: device under test; OTA: over-the-air; V-pol: vertical polarization; H-pol: horizontal polarization

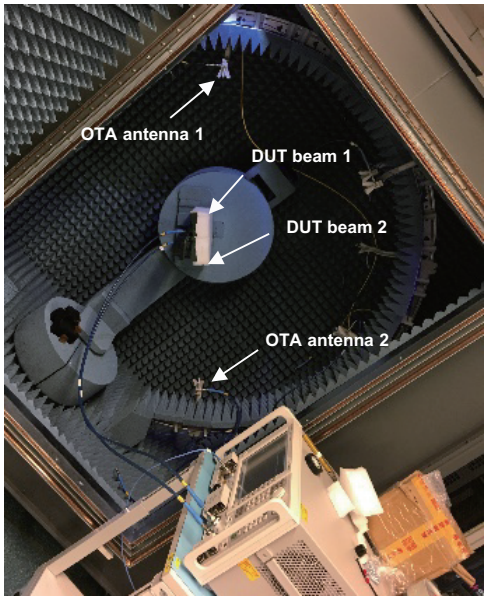

Fig. 6 Measurement setup for the wireless cable method using antenna pattern discrimination
DUT: device under test; OTA: over-the-air

2.4.2 Measurement results

The CIRs measured at the two DUT antennas can be obtained by performing inverse Fourier transform of the CFRs. The measured CIRs for the first and second DUT antennas using the polarization discrimination scheme are shown in Fig. 7. Two taps, with a delay difference of around 935 ns, can be observed in the measured CIRs for the first antenna, with the second tap being around 20 dB smaller than the first one. This basically indicates that the first wireless cable connection is well established, with around −20 dB cross-talk from the second wireless cable connection. We can make similar observations for the second DUT antenna measurement. Note that there is a path difference of around 2.1 dB for the direct link (i.e., the first tap in S_{21} and the second tap in S_{41} measurements). This imbalance should

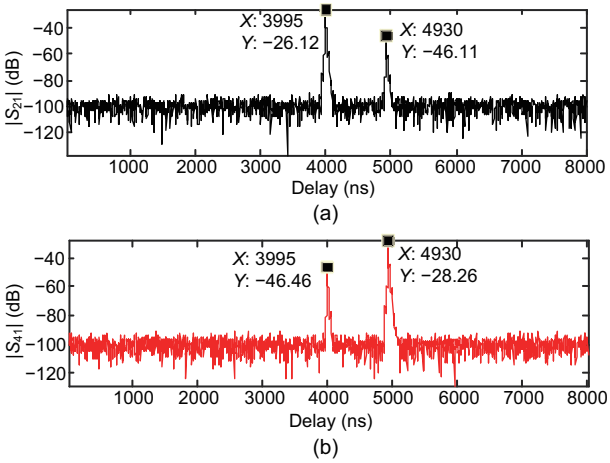

Fig. 7 Measured CIRs for the first (S_{21}) (a) and second (S_{41}) (b) DUT antennas using the polarization discrimination scheme
CIR: channel impulse response; DUT: device under test

be calibrated out in practice to ensure the balanced transmission over wireless cable.

The measured CIRs for the first and second DUT antennas using the antenna pattern discrimination scheme are shown in Fig. 8. As we can see, more than 30 dB isolation can be achieved for both wireless cable connections using this simple scheme.

3 MPAC method

3.1 Principle

The basic idea of the MPAC method is that the signals radiating from the probe antennas are controlled and optimized in the CE such that the reproduced RF environment within the test area mimics the target spatial fading channel (Foegelle, 2014; Fan et al., 2018a). The main advantage of the MPAC method is that it is a true end-to-end testing solution, which can be used to test off-the-shelf DUTs. Unlike the wireless cable method, it works for adaptive DUTs without the need to lock antenna beams during testing. The key assumption is that the DUT would operate as it would in the intended propagation environment, but in a repeatable and controllable way. A simple layout for the MPAC approach is shown in Fig. 9.

The signal model can be written as follows:

$$\begin{aligned}\boldsymbol{y}(f,t) &= \boldsymbol{F}(f,t)\boldsymbol{H}_{\mathrm{CE}}(f,t)\boldsymbol{x}(f,t)\\ &= \hat{\boldsymbol{H}}(f,t)\boldsymbol{x}(f,t),\end{aligned} \tag{3}$$

where $\boldsymbol{H}_{\mathrm{CE}}(f,t)$ is the channel model implemented in the CE, and $\boldsymbol{F}(f,t)$ is the transfer matrix between the OTA probe antenna port and the DUT antenna port. Time-invariant and frequency flat $\boldsymbol{F}$ is often used in the literature, due to the non-adaptive nature of the DUT and the small fractional bandwidths around the carrier frequency. The objective of channel emulation in the MPAC setup is to design $\boldsymbol{H}_{\mathrm{CE}}(f,t)$ in the CE such that $\hat{\boldsymbol{H}}(f,t)$ and $\boldsymbol{H}(f,t)$ are statistically similar (Kyösti et al., 2018). The main challenge lies in reproducing the spatial profile of the fading channels, due to the discrete OTA probe antenna configurations and the limited number of probe antennas, while the other channel parameters (e.g., fading, Doppler profile, and delay characteristics) can be easily reconstructed with the help of a CE. The number of probe antennas required is determined by the spatial discrimination capability of the DUT. Generally speaking, DUTs with a large electric size would offer more directive antenna patterns, which in turn would result in the need for dense sampling, i.e., more probe antennas.

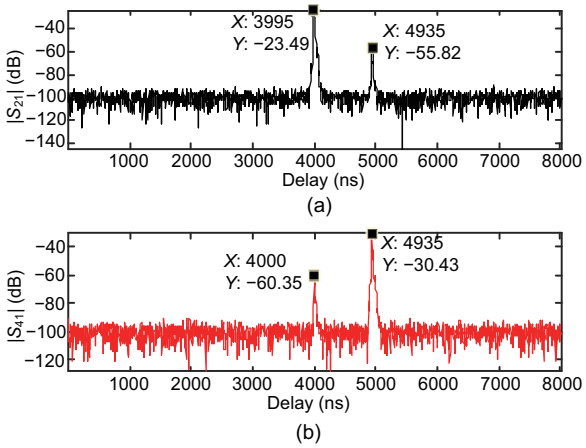

Fig. 8 Measured CIRs for the first (S_{21}) (a) and second (S_{41}) (b) DUT antennas using the beam pattern discrimination scheme

CIR: channel impulse response; DUT: device under test

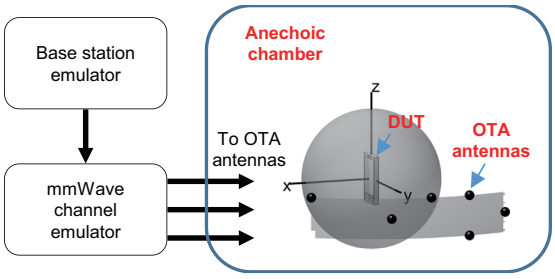

Fig. 9 MPAC system layout for OTA testing of an FR2 MIMO device

DUT: device under test; FR: frequency range; MIMO: multiple-input multiple-output; mmWave: millimetre-wave; MPAC: multi-probe anechoic chamber; OTA: over-the-air

3.2 Applicability for mmWave NR

The MPAC method has been standardized for 4G mobile handset testing in the 2×2 downlink MIMO and transmit diversity modes (CTIA, 2017). For the MPAC configuration, eight dual-polarized probe antennas (which are connected to 16 CE RF interface ports) are placed on a 2D OTA ring. This is mainly due to the fact that the 2D spatial channel models, i.e., spatial channel model extended (SCME) urban macro (UMa) and SCME urban micro (UMi), are assumed to be sufficient for performance testing. A uniform probe configuration also has the benefit of offering flexibility to emulate arbitrary spatial channel profiles. The supported test zone size is around 0.8λ, where λ is the wavelength.

For MIMO OTA testing of 5G radios, the MPAC setup configurations are different in FR1 and FR2. In FR1, 16 uniformly distributed dual-polarized probe antennas are used on a 2D OTA ring. This can be seen as a direct extension from the 4G MPAC setup. The channel models are simplified 2D versions of the 3GPP 38.901 channel models (i.e., ignoring the elevation dimension) (3GPP, 2020). The required number of probe antennas is doubled to support a large test zone (in terms of electrical size), due to the high operating frequency in FR1 (e.g., up to 5 GHz) compared to 4G LTE bands.

However, for 5G handsets operating at FR2, a different MPAC configuration is adopted due to several reasons (3GPP, 2020). Thus, 3D spatial channel modeling is seen as essential to enabling 3D beam steering for mmWave antenna systems. Furthermore, the test zone size (in terms of electrical size) is significantly large for mmWave systems, which would necessitate a massive number of OTA antennas and associated CE resources. Therefore, the main challenge for MPAC design in mmWave bands is to reduce the system cost yet still ensuring realistic fading channels for performance testing. A simple 3D sectored MPAC setup, which consists of six dual-polarized probe antennas, is adopted, as shown in Fig. 9 (3GPP, 2020). The simple 3D MPAC setup, though limited in terms of flexibility in emulating arbitrary channel models, has been proven to be capable of emulating two representative 3D channel models over a large test area (3GPP, 2020).

3.3 Measurement setup

The system diagram of the measurement setup for validating the MPAC solution is shown in Fig. 10. The VNA transmits the signals through the CE and the probe antennas. The three probes radiate the faded signals within the anechoic chamber, and a receiving test antenna is placed within the test zone. The test antenna is attached to a positioner on the turntable that can move the antenna to predefined spatial locations. The received signals are then recorded with the VNA. The vertically polarized antenna feeds of the three probe antennas are connected to the mmWave CE. Three narrowband time-variant channel models are loaded in the CE, with average power of 0, −3, and −10 dB, respectively. The loaded channel profiles $h_1(t)$, $h_2(t)$, and $h_3(t)$ follow independent and identical distributions (i.i.d.) (complex normal distributions). Accordingly, 10 000 channel snapshots are realized for each faded channel profile, with four samples per wavelength sampling density (3GPP, 2020).

A graphical representation of the practical measurement system is shown in Fig. 11. Three dual-polarized probe antennas are on the same ring with an angle separation of 60°. A vertically polarized biconical antenna (Fan et al., 2016) with an omni-

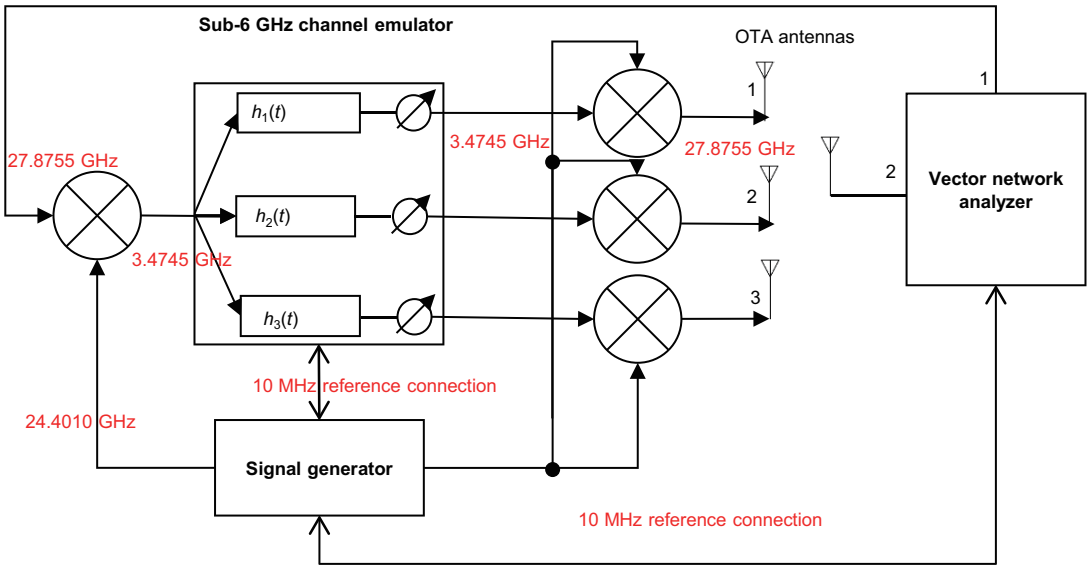

Fig. 10 System diagram for the SS-MPAC setup

OTA: over-the-air; SS-MPAC: simple sectored multi-probe anechoic chamber

directional antenna pattern in the azimuth plane (i.e., OTA ring) is selected as the test antenna. A virtual linear array in the OTA ring plane is formed by a mechanical linear slide. The virtual array concept is adopted to measure the spatial profile of the emulated channel inside the chamber. Basically, the biconical antenna is moved to 16 predefined locations (i.e., [0, 0.2, 0.4, 0.6, 0.8, 1.0, 1.4, 1.8, 2.2, 2.6, 3.0, 3.4, 3.8, 4.2, 4.6, 5.0]λ at f_c=27.876 GHz). Note that the measured locations are smaller than 0.5λ to avoid the spatial aliasing problem in the PAS estimation. The measurement step is as small as 0.2λ (corresponding to around 2 mm), which demands a highly accurate positioning system. For channel validation in sub-6 GHz MIMO OTA testing, a spacing of 0.1λ was selected (i.e., 1 cm at 3 GHz). In our experimental validation, spacings of 0.2λ and 0.4λ were selected. Note that the physical spacing in the mmWave case is required to be much smaller, i.e., around 2 mm in our measurement compared to 1 cm at 3 GHz. Note that as long as the spatial sampling spacing is smaller than 0.5λ, we can fully capture the spatial characteristics of the channel in the test zone. For each position of the test antenna, we can step and pause the process in the CE to different channel snapshots. Then the CFRs are measured for all stepped channel snapshots. The number of channel snapshots is set to 1000 (i.e., every 10 channel snapshots to ensure independent channel snapshots) and the number of frequency samples is set to 1 (i.e., zero span frequency setting in the VNA). We can then repeat the steps to record the CFRs for all the 16 spatial sample points.

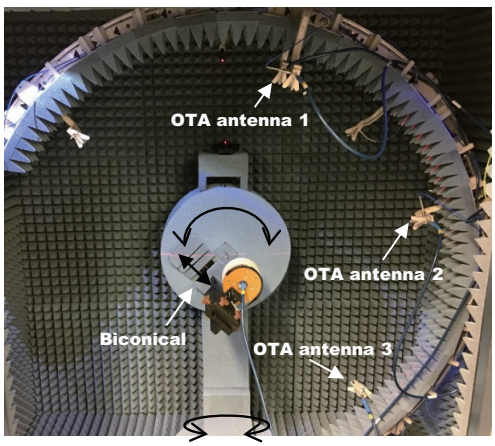

Fig. 11 System diagram for the MPAC setup
MPAC: multi-probe anechoic chamber; OTA: over-the-air

3.4 Measurement results

3.4.1 Spatial correlation

The signals received at the elements of the virtual array (i.e., spatial locations) can be written in a matrix form as follows:

$$\boldsymbol{r}[t] = \boldsymbol{F}\boldsymbol{s}[t] + \boldsymbol{v}[t], \tag{4}$$

where $\boldsymbol{r}[t] \in \mathbb{C}^{N\times 1}$ is a vector containing N received signals at the t^{th} snapshot for $t \in [1, T]$, with $T = 1000$. $\boldsymbol{F} \in \mathbb{C}^{N\times K}$ is a transfer function matrix of coefficients from the k^{th} probe to the n^{th} test antenna, which can be simplified by the free-space propagation formula. $\boldsymbol{s}[t] \in \mathbb{C}^{K\times 1}$ is a vector containing K transmitted signals at the t^{th} snapshot, which is known beforehand. $\boldsymbol{v}[t] \in \mathbb{C}^{N\times 1}$ is a noise vector, which can be ignored in the validation measurement in the anechoic chamber due to good dynamic range of the signal.

The autocovariance $\hat{\boldsymbol{R}} \in \mathbb{C}^{N\times N}$ of the received signals can be calculated as follows:

$$\hat{\boldsymbol{R}} = \frac{1}{T}\sum_{t} \boldsymbol{r}[t]\boldsymbol{r}^{\text{H}}[t]. \tag{5}$$

The spatial correlation coefficients among the elements of the virtual array are the entries from the normalized autocovariance matrix. The measured spatial correlation result is shown in Fig. 12. As we can see, the measured spatial correlation result matches well with the target one. The small deviation might be introduced by the limited number of time snapshots, the position accuracy of the practical system, the probe configuration accuracy, and so on.

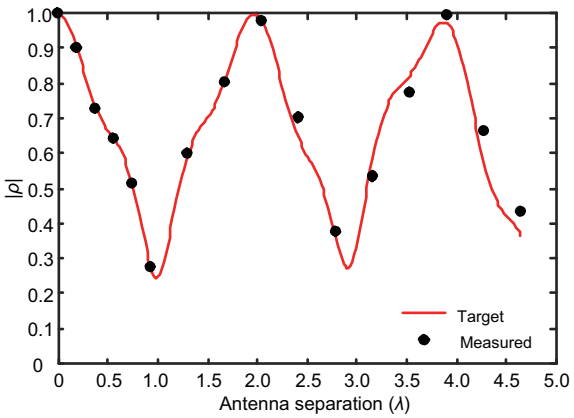

Fig. 12 Measured and target spatial correlation in the MPAC setup

3.4.2 PAS estimate

The PAS estimate can be obtained from the following expression:

$$\hat{P}(\phi) = \boldsymbol{a}^{\mathrm{H}}(\phi)\hat{\boldsymbol{R}}\boldsymbol{a}(\phi), \tag{6}$$

where $\boldsymbol{a}(\phi) \in \mathbb{C}^{N\times 1}$ is the array steering vector of the virtual linear array to the angle ϕ. The measured and target PASs in the MPAC setup are shown in Fig. 13. Three peaks can be clearly observed in the measured spectrum. The peak power values, normalized to the first peak, are 0, −3, and −10.3 dB, indicating excellent agreement with the target values. The peak angles are 0°, 61°, and 123°, which also agree well with the target values.

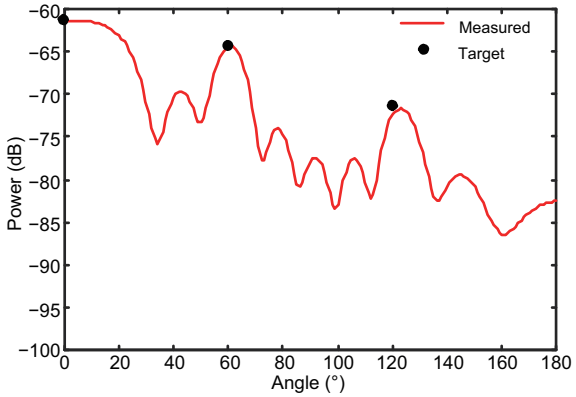

Fig. 13 Measured and target power angular spectrum in the MPAC setup

MPAC: multi-probe anechoic chamber

4 Conclusions

The use of mmWave technology is of vital importance to the design, development, and evaluation of 5G communication systems. The focus of this paper is on spatial channel emulation in the anechoic chamber for OTA performance testing of mmWave radios. Two OTA methods have been investigated for mmWave radios with preliminary experimental results, namely the wireless cable method and the MPAC method. The measurement has been carried out in an FR2 chamber, which has not been reported yet in the literature. Three strategies to achieve wireless cable connection have been discussed, i.e., transfer function matrix calibration, polarization discrimination, and antenna pattern discrimination. It is shown in the preliminary measurement results at around 28 GHz that an isolation more than 20 dB and 30 dB can be achieved for the wireless cable method using polarization discrimination and antenna pattern discrimination, respectively. In other words, a good wireless cable connection could be easily established for 2 × 2 MIMO FR2 systems. We have also pointed out that transfer function matrix calibration is a more generic strategy for the wireless cable method which works for all scenarios. The spatial correlation and PAS have also been investigated for a simple MPAC setup in the FR2 chamber. Excellent agreement between the measurement results and the target values is achieved in terms of spatial correlation and PAS, which validates the effectiveness of the MPAC method in the mmWave bands. The work experimentally validates the applicability of the wireless cable method and the MPAC method in the mmWave NR testing scenario, which will be a valuable input to the ongoing 3GPP standardization process.

Contributors

Wei FAN designed the research, performed the measurement, and drafted the manuscript. Lassi HENTILÄ helped perform the measurement. Pekka KYÖSTI helped design the research and organize the manuscript. Wei FAN revised and finalized the paper.

Compliance with ethics guidelines

Wei FAN, Lassi HENTILÄ, and Pekka KYÖSTI declare that they have no conflict of interest.

References

3GPP, 2019. Study on Test Methods.

3GPP, 2020. Study on Radiated Metrics and Test Methodology for the Verification of Multi-antenna Reception Performance of NR User Equipment (UE).

Chen XM, 2014. Throughput modeling and measurement in an isotropic-scattering reverberation chamber. *IEEE Trans Antenn Propag*, 62(4):2130-2139. https://doi.org/10.1109/TAP.2014.2301850

Chen XM, Kildal PS, Orlenius C, et al., 2009. Channel sounding of loaded reverberation chamber for over-the-air testing of wireless devices: coherence bandwidth versus average mode bandwidth and delay spread. *IEEE Antenn Wirel Propag Lett*, 8:678-681. https://doi.org/10.1109/LAWP.2009.2025149

CTIA, 2017. Test Plan for 2 × 2 Downlink MIMO and Transmit Diversity Over-the-Air Performance. CTIA, Washington, USA.

CTIA, 2018. Test Plan for Mobile Station Over-the-Air Performance: Method of Measurement for Radiated RF Power and Receiver Performance.

Fan W, Carton I, Nielsen JØ, et al., 2016. Measured wideband characteristics of indoor channels at centimetric and millimetric bands. *EURASIP J Wirel Commun Netw*, 2016(1):58. https://doi.org/10.1186/s13638-016-0548-x

Fan W, Kyösti P, Hentilä L, et al., 2017. MIMO terminal performance evaluation with a novel wireless cable method. *IEEE Trans Antenn Propag*, 65(9):4803-4814. https://doi.org/10.1109/TAP.2017.2723260

Fan W, Kyösti P, Hentilä L, et al., 2018a. A flexible millimeter-wave radio channel emulator design with experimental validations. *IEEE Trans Antenn Propagat*, 66(11):6446-6451. https://doi.org/10.1109/TAP.2018.2864339

Fan W, Kyösti P, Rumney M, et al., 2018b. Over-the-air radiated testing of millimeter-wave beam-steerable devices in a cost-effective measurement setup. *IEEE Commun Mag*, 56(7):64-71. https://doi.org/10.1109/MCOM.2018.1701006

Foegelle MD, 2014. The future of MIMO over-the-air testing. *IEEE Commun Mag*, 52(9):134-142. https://doi.org/10.1109/MCOM.2014.6894464

Guan K, Peng BL, He DP, et al., 2019a. Channel characterization for intra-wagon communication at 60 and 300 GHz bands. *IEEE Trans Veh Technol*, 68(6):5193-5207. https://doi.org/10.1109/TVT.2019.2907606

Guan K, Peng BL, He DP, et al., 2019b. Measurement, simulation, and characterization of train-to-infrastructure inside-station channel at the terahertz band. *IEEE Trans Terahertz Sci Technol*, 9(3):291-306. https://doi.org/10.1109/TTHZ.2019.2909975

Ji YL, Fan W, Nilsson MG, et al., 2020. Virtual drive testing over-the-air for vehicular communications. *IEEE Trans Veh Technol*, 69(2):1203-1213. https://doi.org/10.1109/TVT.2019.2956571

Jing Y, Kong HW, Rumney M, 2016. MIMO OTA test for a mobile station performance evaluation. *IEEE Instrum Meas Mag*, 19(3):43-50. https://doi.org/10.1109/MIM.2016.7477954

Keysight Technologies, 2018. OTA Test for Millimeter-Wave 5G NR Devices and Systems.

Kyösti P, Hentilä L, Fan W, et al., 2018. On radiated performance evaluation of massive MIMO devices in multiprobe anechoic chamber OTA setups. *IEEE Trans Antenn Propag*, 66(10):5485-5497. https://doi.org/10.1109/TAP.2018.2860635

Li Y, Xin LJ, Liu XQ, et al., 2020. Dual anechoic chamber setup for over-the-air radiated testing of 5G devices. *IEEE Trans Antenn Propag*, 68(3):2469-2474. https://doi.org/10.1109/TAP.2019.2943360

Muruganathan SD, Lin XQ, Maattanen HL, et al., 2018. An overview of 3GPP Release-15 study on enhanced LTE support for connected drones. https://arxiv.org/abs/1805.00826

Nilsson MG, Hallbjörner P, Arabäck N, et al., 2015. Measurement uncertainty, channel simulation, and disturbance characterization of an over-the-air multiprobe setup for cars at 5.9 GHz. *IEEE Trans Ind Electron*, 62(12):7859-7869. https://doi.org/10.1109/TIE.2015.2475423

Qi YH, Yang G, Liu L, et al., 2017. 5G over-the-air measurement challenges: overview. *IEEE Trans Electromagn Compat*, 59(6):1661-1670. https://doi.org/10.1109/TEMC.2017.2707471

Qiao ZL, Wang ZP, Fan W, et al., 2020. Low scattering plane wave generator design using a novel non-coplanar structure for near-field over-the-air testing. *IEEE Access*, 8:211348-211357. https://doi.org/10.1109/ACCESS.2020.3039367

Rappaport TS, Sun S, Mayzus R, et al., 2013. Millimeter wave mobile communications for 5G cellular: it will work! *IEEE Access*, 1:335-349. https://doi.org/10.1109/ACCESS.2013.2260813

Rumney M, 2016. Testing 5G: time to throw away the cables. *Microw J*, 59(11):10-12,14,16,18.

Rumney M, Kong HW, Jing Y, et al., 2016. Recent advances in the radiated two-stage MIMO OTA test method and its value for antenna design optimization. Proc 10th European Conf on Antennas and Propagation, p.1-5. https://doi.org/10.1109/EuCAP.2016.7481105

Schirmer C, Lorenz M, Kotterman ATT, et al., 2016. MIMO over-the-air testing for electrically large objects in non-anechoic environments. Proc 10th European Conf on Antennas and Propagation, p.1-6. https://doi.org/10.1109/EuCAP.2016.7481106

Shafi M, Molisch AF, Smith PJ, et al., 2017. 5G: a tutorial overview of standards, trials, challenges, deployment, and practice. *IEEE J Sel Areas Commun*, 35(6):1201-1221. https://doi.org/10.1109/JSAC.2017.2692307

Wang WM, Wang RR, Gao HQ, et al., 2019. Implementation and analysis of 3D channel emulation method in multi-probe anechoic chamber setups. *IEEE Access*, 7:108571-108580. https://doi.org/10.1109/ACCESS.2019.2933494

Yu W, Qi YH, Liu KF, et al., 2014. Radiated two-stage method for LTE MIMO user equipment performance evaluation. *IEEE Trans Electromagn Compat*, 56(6):1691-1696. https://doi.org/10.1109/TEMC.2014.2320779

Zhang FC, Fan W, Wang ZP, 2021. Achieving wireless cable testing of high-order MIMO devices with a novel closed-form calibration method. *IEEE Trans Antenn Propag*, 69(1):478-487. https://doi.org/10.1109/TAP.2020.3008647

Zhang YS, Wang ZP, Sun XL, et al., 2020. Design and implementation of a wideband dual-polarized plane wave generator with tapered feeding nonuniform array. *IEEE Antenn Wirel Propag Lett*, 19(11):1988-1992. https://doi.org/10.1109/LAWP.2020.3010118